Statistical characterization of thermal plumes in turbulent thermal convection

Sheng-Qi Zhou (周生启),[1,2] Yi-Chao Xie (谢毅超),[1] Chao Sun (孙超),[1,3] and Ke-Qing Xia (夏克青)[1,*]

[1]*Department of Physics, The Chinese University of Hong Kong, Shatin, Hong Kong, China*

[2]*State Key Laboratory of Tropical Oceanography, South China Sea Institute of Oceanology, Chinese Academy of Sciences, Guangzhou 510301, China*

[3]*Center for Combustion Energy and Department of Thermal Engineering, Tsinghua University, Beijing 100084, China*

(Received 9 June 2016; published 12 September 2016)

We report an experimental study on the statistical properties of the thermal plumes in turbulent thermal convection. A method has been proposed to extract the basic characteristics of thermal plumes from temporal temperature measurement inside the convection cell. It has been found that both plume amplitude A and cap width w, in a time domain, are approximately in the log-normal distribution. In particular, the normalized most probable front width is found to be a characteristic scale of thermal plumes, which is much larger than the thermal boundary layer thickness. Over a wide range of the Rayleigh number, the statistical characterizations of the thermal fluctuations of plumes, and the turbulent background, the plume front width and plume spacing have been discussed and compared with the theoretical predictions and morphological observations. For the most part good agreements have been found with the direct observations.

DOI: 10.1103/PhysRevFluids.1.054301

I. INTRODUCTION

Turbulent thermal convection plays a vital role in the dynamics of systems such as the Earth's atmosphere, oceans, its mantle, and in the interior of astrophysical objects such as planets and stars [1,2]. It is also an important mechanism for heat transfer in many engineering applications. The turbulent Rayleigh-Bénard convection (RBC), which is a fluid layer confined between two horizontally parallel conducting plates heated from below and cooled from above, is arguably the simplest system to model the various convection phenomena. The RBC has three control parameters: the Rayleigh number $\mathrm{Ra} = \alpha g \Delta T H^3/(\nu\kappa)$, the Prandtl number $\mathrm{Pr} = \nu/\kappa$, and the aspect ratio $\Gamma = D/H$, with g being the gravitational acceleration constant, ΔT the applied temperature difference across a fluid layer of height H and lateral size D, and α, ν, and κ, respectively, the thermal expansion coefficient, the kinematic viscosity, and the thermal diffusivity of the working fluid. Turbulent RBC has attracted much attention in the past three decades partially due to its convenience to study dynamics of coherent structures and organised flows, e.g., thermals, plumes, and large-scale circulation (LSC), over a turbulent background flow [3–7]. It has been shown that thermal plumes, as the most important coherent structure in turbulent RBC, play a crucial role in driving the LSC and in carrying heat across the convection cell [8–10].

The importance of thermal plumes in convective turbulence has been recognized about a half century ago [11,12]. Zocchi, Moses, and Libchaber described the "life cycle" of plumes and other coherent structures in the system [13]. To look for the statistical signatures of plumes from the measured temperature time series, Belmonte and Libchaber studied the skewness of the temperature time derivative and concluded that temperature in turbulent convection behaves as an active scalar [14]. To directly explore their properties, Zhou and Xia extracted plumes as individual objects from the measured temperature signal in turbulent RBC using a method similar to that used in identifying

*Corresponding author: kxia@phy.cuhk.edu.hk

fronts in passive scalars [15]. They found that both the amplitude and width of thermal plumes have log-normal distributions, which are, surprisingly, similar to what has been found for passive scalars. These experimental results indicated that, as active scalars, plumes possess statistical properties similar to passive scalars. In a numerical study, Julien *et al.* identified individual plumes by applying a threshold to each of the temperature, vertical velocity, and vertical vorticity fields [16]. Based on the fact that, as buoyant objects, the temperature and vertical velocity of plumes should be correlated in some way, Ching *et al.* extracted thermal plume using the conditional average of velocity on temperature from the simultaneously measured local velocity and temperature signals [17]. In a numerical study, Shishkina and Wagner extracted thermal plumes by associating these objects with the large thermal dissipation rates [18,19]. Based on the fact that temperature of thermal plumes should be larger (smaller) than the surrounding fluid for a hot (cold) plume, Huang *et al.* and Xie *et al.* developed a conditional averaged method to identify thermal plumes [20,21].

In addition to the studies of the statistical properties of thermal plumes, their morphology in turbulent RBC also became a subject of interest recently. It has long been observed that thermal plumes take a mushroom-like shape in the bulk of the convection cell [8,9,13,22]. In a shadowgraphic study, however, Funfschilling and Ahlers found that plumes are sheetlike objects around the boundary layer [23]. To understand the position-dependent morphologies of thermal plumes in turbulent RBC, Zhou, Sun, and Xia studied the geometrical properties of the thermal plumes using thermochromic liquid crystal microspheres [24]. Their study revealed how sheetlike plumes change into mushroom-like ones through a morphological transformation when they are moving away from the boundary layer region into the bulk flow. In a later study over a wider Ra range, Zhou and Xia further characterized the geometrical and statistical properties of thermal plumes [25]. In a shadow-graph measurement, Bosbach, Weiss, and Ahlers found that thermal plumes underneath the top plate undergo fragmentation process arising from the interactions of the plume with bulk fluctuations or up-welling domain walls [26].

Apart from being individual objects, thermal plumes also cluster together in their migration across the convection cell. From flow visualization and local temperature measurements, Qiu and Tong observed that plumes near the sidewall region often move in groups [27,28]. To pinpoint how plumes organize themselves and drive the LSC, Xi, Lam, and Xia studied the onset of the LSC in turbulent RBC using shadow-graph and particle-image velocimetry (PIV) techniques [8]. They found that the grouping or clustering of plumes arises from the interaction between the small vortices generated by the individual plume, and the clustered plumes in turn generate large vortices that lead to the formation of the LSC spanning the entire convection cell. Thus, it is the clustered plumes that are mainly responsible for driving the LSC or the "wind" in turbulent thermal convection. Clustering of thermal plumes has also been found in numerical studies of turbulent RBC [29,30]. In addition, Bershadskii *et al.* have introduced a "telegraph" method to quantify the clustering of plumes from measured temperature time series [31]. A consequence of the plume clustering is that heat transport across the convection cell becomes highly inhomogeneous both spatially and temporally. As demonstrated by Shang *et al.*, the local heat flux across the convection cell is predominately transported by thermal plumes near the sidewall with quasi-time-periodic bursts [9,10]. Partly motivated by these developments, Grossmann and Lohse treated the role of plumes explicitly in a model taking into fluctuations for turbulent thermal convection [32–35], in which the contributions to the thermal dissipation by plumes and by the turbulent "background" are considered separately [35]. In their model, the temperature fluctuations related to thermal plumes and background fluctuations are predicted to have different scalings with respect to Ra and Pr.

Although the thermal plumes can be studied in visualization experiments and direct numerical simulations (DNSs) [24,25,36–38], to quantitatively determine some of their statistical properties would require a large data set or long time record, which are not easy to obtain from either the visualization experiments or DNS studies. This makes the local temperature measurement a suitable method to study the long time statistics of thermal plumes.

The remainder of the paper is organized as follows. In Sec. II we describe the convection cell and temperature measurements and introduce the plume extraction method. In Sec. III we first

present the statistical properties of thermal plumes at the local positions for a fixed Rayleigh number $\mathrm{Ra} = 1.85\times10^{10}$. Then we discuss the Ra dependence of various plume quantities. A brief summary is given in Sec. IV.

II. EXPERIMENTAL SETUP AND PLUME EXTRACTION METHOD

A. Experimental setup and measurement techniques

The experimental setup has been described elsewhere [39]; here we give key features of the convection cell and the temperature measurements. As shown in Fig. 1, the convection cell was a cylindrical Plexiglas tube 19.0 cm in diameter D and 19.6 cm in height H (the aspect ratio $\Gamma = \frac{D}{H}$ was hence approximately unity). The surfaces of the top and bottom copper plates were gold-plated. The temperature of the top plate was regulated by passing cold water through a chamber fitted on its top. The bottom plate was heated with an embedded film heater. The temperature difference ΔT between the two plates was monitored by four thermistors embedded inside the plates. By varying temperatures of both plates, we were able to vary Ra from 2.0×10^{8} to 1.85×10^{10} while keeping Pr at 4.3. The measured relative temperature difference between any two thermistors in the same plate was less than 1% for all Ra. The temperature fluctuations of either plate varied from 0.2% to 4% of ΔT for high and low values of Ra. The convection cell was packaged with thermal insulation and was placed inside a thermostat box, where the temperature was set to match the mean temperature of the working fluid to minimize the influence of ambient temperature fluctuations.

Local temperature in fluid was measured by two small thermistors with a diameter of $\sim100\,\mu$m and a time constant of 5 ms in water (Model AB6E3-B05, Thermometrics Inc). One thermistor was located at the midheight of the convection cell and $x = 20$ mm away from the sidewall (Point A in Fig. 1), which is referred to as the sidewall measurement hereafter. The other thermistor was located at the central symmetric line of the cylindrical convection cell and $z = 20$ mm above the bottom plate (Point B in Fig. 1), which is referred as the bottom plate measurement. Each thermistor had a separate measurement system consisting of an AC Wheatstone bridge and a lock-in amplifier [39]. The output signals from the lock-in amplifiers were digitized by a multiple-channel dynamic signal analyzer (HP35670A) with the sampling rate varied from 16 to 128 Hz with increasing Ra. The measurement lasted from 9 to 18 h with decreasing Ra. In total, 1 to 4 million data were collected. In addition, two extra-long temperature measurements were carried out at both positions at $\mathrm{Ra} = 1.85\times10^{10}$ with a sampling rate of 128 Hz; each contained 1.2×10^{8} data.

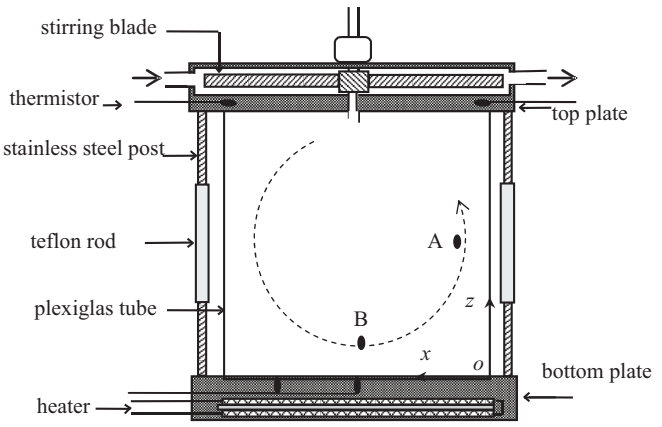

FIG. 1. Schematics of the convection cell and the coordinates for the experiment. The large-scale circulation (LSC) is sketched as the dashed line. Two thermistors were used to measure local temperatures within the LSC plane, one located at position A, in the midheight of the cell, and $x = 20$ mm away from the sidewall, the other one located at position B, in the central symmetric line $z = 20$ mm above the bottom plate.

B. Plume extraction algorithm

Before introducing the plume extraction method, let us first look at a typical plume evolved from a point heater as shown in the inset of Fig. 2(a). It consists of a clear cap and a weak stem following it. The cap was generated due to the sharp temperature or density difference with the surrounding fluids. The stem provides thermal energy to the cap from the heater [40,41]. When the plume transits a thermistor above it, a cliff-ramp structure was captured in the temperature signal, as shown in Fig. 2(a). The sharp "cliff" corresponds to the plume cap and the "ramp" to its stem.

In the case of turbulent thermal convection, thermal plumes will interact with each other and with the turbulent background flow inside the convection cell. Consequently, they are stretched, knotted, and deformed. This interaction leads to the formation of either mushroom-like or sheetlike thermal plumes [23,24]. However, some of the characteristics of the thermal plumes retain in the case of turbulent thermal convection. One such characteristic is the typical cliff-ramp structure which remains unchanged due to the sharp temperature gradient. To extract the information of the thermal plumes, e.g., the cliff-ramp structure, from the turbulent temperature signals, we use a three-step algorithm described below.

Step 1: We determine the time position t_0 [see Fig. 2(a)] of a thermal plume. Based on the cliff-ramp shape of the temperature profile generated from a thermal plume, t_0 is identified when a temperature increment satisfies the criterion:

$$\delta T(t) > \beta T_{\mathrm{rms}}. \tag{1}$$

Here $\delta T(t) = [T(t+\tau) - T(t)]$ is the temperature increment over a time interval τ at time t, where τ is usually related to the sampling rate f_0; e.g., it is $4/f_0$ at $f_0 = 128$ Hz. β is a threshold and $T_{\mathrm{rms}} = \langle (T - \langle T \rangle)^2 \rangle^{1/2}$ is the root-mean-square (rms) temperature with $\langle \cdots \rangle$ denoting the time average. Since the plume cap has the largest temperature contrast with the surrounding fluid, it is thus reasonable to take the position of the maximum temperature increment as the time position of thermal plume. In the case where the temperature increments match the criterion [see, e.g., Eq. (1)] in several successive times, the time of maximum temperature increment is then taken as t_0.

Step 2: To capture the character of plume cap, we track the other two time positions of temperature extrema t_1 and t_2 around t_0 with $t_1 < t_0$ and $t_2 > t_0$. For example, in the case of a hot plume, t_1 and t_2 correspond to the positions of the local minimum and maximum temperatures [see, e.g., Fig. 2(a)]. The time interval between t_1 and t_2 represents the transit time for the cap passing through the thermistor, which is defined as the plume width $w = t_2 - t_1$. Correspondingly, the absolute value of the temperature difference between the positions $A = |T(t_2) - T(t_1)|$ is defined as the plume amplitude.

Step 3: To discriminate the cliff-ramp-like plume signal as argued in Ref. [42], the average temperature at t_1 and t_2, i.e., $[T(t_1) + T(t_2)]/2$, needs to be larger (smaller) than the average temperature for hot (cold) plumes is applied. Time traces that cannot fulfill the criterion in this step are thus discarded.

Examples of the extracted plume signals are shown in Figs. 2(b) and 2(c) (note that these two figures have been shown in Ref. [6] and are reproduced here for ease of reference). Figure 2(b) shows the cold plumes extracted from the temperature data near the top plate at $\mathrm{Ra} = 5.4\times10^9$, and Fig. 2(c) shows the hot plumes extracted near the bottom plate at $\mathrm{Ra} = 1.85\times10^{10}$. It is seen that the cliff-ramp-like structures are evident in the representations of thermal plumes. However, the "ramp" part of these structures does not seem as significant as that observed in Fig. 2(a). The reason is that the plume stem has a weak temperature gradient that can be affected easily by the background temperature fluctuations.

Finally, we have checked the efficiency of the plume extraction method. We directly count the number of cliff-ramp structures in a half-hour temperature time trace measured near the bottom plate at $\mathrm{Ra} = 1.85\times10^{10}$. It is found that about 80% of the cliff-ramp structures have been identified when $\beta = 0.55$ is chosen in the method. Since the cliff-ramp-like structures are very common in turbulent flows, e.g., they are observed in the chemical plume [43], the thickness fluctuations in

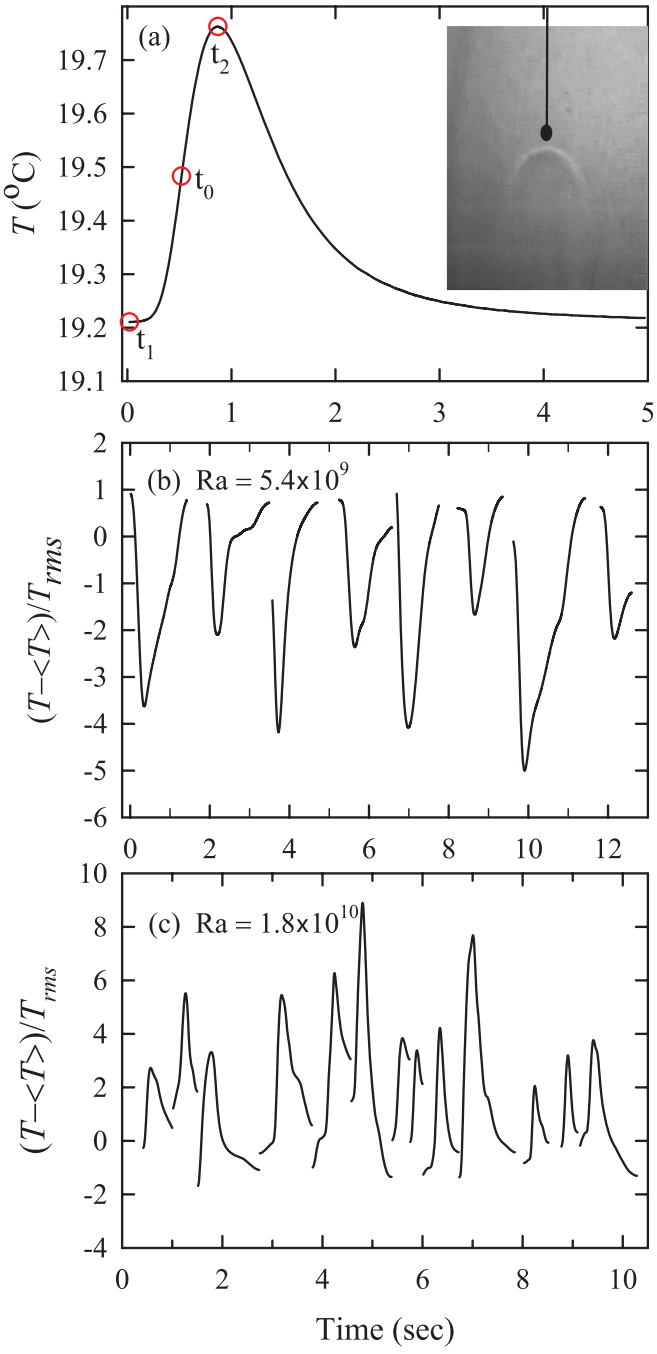

FIG. 2. (a) Temperature signal captured from a laminar plume. t_0, t_1, and t_2 denote the time positions of the maximum temperature increment, the minimum temperature, and the maximum temperature, respectively. Inset: Laminar plume produced from a point heat source. (b) Temperature signal of cold plumes extracted near the top plate at $\mathrm{Ra} = 5.4\times10^9$. (c) Temperature signal of hot plumes extracted near the bottom plate at $\mathrm{Ra} = 1.8\times10^{10}$. Panels (b) and (c) are adopted from Ref. [6].

liquid films [44], the passive scalar turbulence [45–48], and so on, this method might have more broad applications.

III. RESULTS AND DISCUSSION

A. Statistical properties of thermal plumes at Ra = 1.85×10^{10}

As reported in previous work, both the amplitude A and the plume width w have log-normal distributions, as do their product [15]. Here we will examine whether the distribution is affected by the threshold value β.

By applying the plume extraction method to the extra-long temperature time traces measured at Ra = 1.85×10^{10}, we obtain plume amplitude A and plume width w at $\beta = 0.4$, 1.2, and 2.0. We first examine the results measured near the bottom plate. Due to the presence of the horizontal large-scale flow and the buoyant force, the plumes detected here are mainly initiated from the bottom thermal boundary layer and tend to flow in a tilted direction with respect to gravity. Figures 3(a) and 3(b) show the histograms of the normalized plume amplitude $A/T_{\rm rms}$ and its log-form $\log(A/T_{\rm rms})$, respectively. The mean amplitudes $\langle A\rangle$ are found to be 2.95 $T_{\rm rms}$, 5.82 $T_{\rm rms}$, and 8.82 $T_{\rm rms}$ for $\beta = 0.4$, 1.2, and 2.0, respectively. The increase of the mean plume amplitude is also reflected by the histograms shown in Fig. 3(a) where the most probable plume amplitude of the plumes shifts to higher values with increasing β. This can be understood as that the weak plumes are excluded at larger values of β. Nevertheless, the shape of histogram remains self-similar at different values of β, as shown in Fig. 3(b). All histograms are close to log-normal distributions with the right tails slightly stretched. The normalized most probable plume width w_p/τ_0 remains approximately the

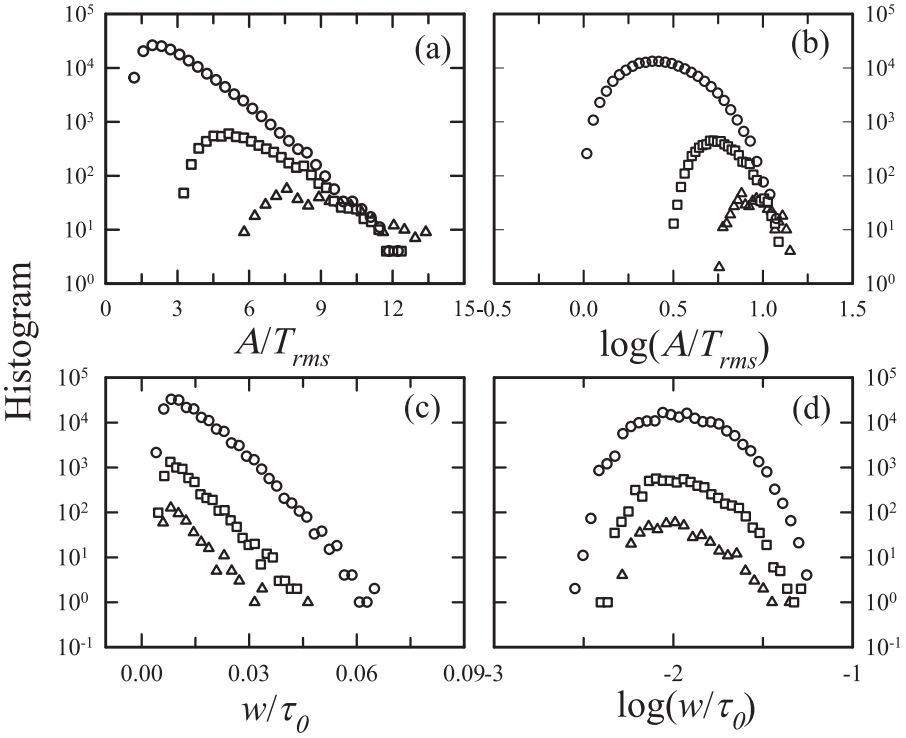

FIG. 3. Histograms of (a) the normalized plume amplitude $A/T_{\rm rms}$ and (b) its log form, (c) normalized plume width w/τ_0, and (d) its log form extracted using temperature time series measured near the bottom plate (at $z = 20$ mm) at $\beta = 0.4$ (circles), 1.2 (squares), and 2.0 (triangles).

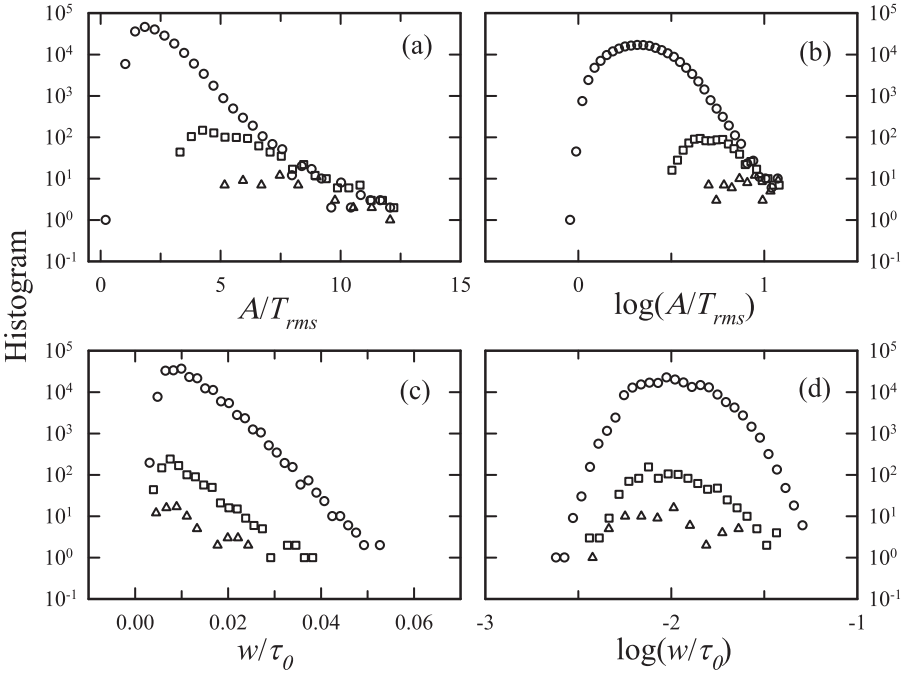

FIG. 4. Histograms of (a) the normalized plume amplitude $A/T_{\rm rms}$ and (b) its log form, (c) the normalized plume width w/τ_0, and (d) its log form extracted from the temperature time series measured near the sidewall (at $x = 20$ mm) at $\beta = 0.4$ (circles), 1.2 (squares), and 2.0 (triangles).

same ($\approx 0.01\tau_0$) for the three values of β, as shown in Fig. 3(c), suggesting that w_p is a typical time scale of thermal plumes that is independent of β. Here τ_0 is the large-scale circulation turnover time. As shown in Fig. 3(d), the histogram of w/τ_0 is also in a well-shaped log normal distribution.

Near the sidewall, we get qualitatively similar results of A and w as those near the bottom plate for $\beta = 0.4, 1.2$, and 2.0. Shown in Figs. 4(a) and 4(b) are the histograms of plume amplitude and its log-form for different values of β. The only difference when compared to measurements near the bottom plate is that A is more skewed towards positive values near the sidewall, and its distribution is more similar to that observed in the passive scalar [48]. The histograms of normalized plume width w/τ_0 and its log form $\log(w/\tau_0)$ are shown in Figs. 4(c) and 4(d), respectively. Similar to the observations near the bottom plate, the histogram of w/τ_0 peaks around $0.01\tau_0$, and it is in a well-shaped log-normal distribution [Fig. 4(d)].

The above results thus suggest that the log-normal distribution of plume amplitude and width is independent of the measurement location and the threshold β used in the plume extraction method. This distribution is an intrinsic feature of thermal plumes in turbulent thermal convection. In morphological measurements, it is also found that the area of thermal plumes and the plume spacing have log-normal distributions [24,38].

The time interval between two successive plumes, donated as τ_v, is another important aspect of thermal plumes. When multiplied by the typical velocity of thermal plumes, it represents the plume spacing. In Fig. 5 we show the histogram of the normalized time interval between plumes τ_v/τ_0 near both the bottom plate and the sidewall at $\beta = 0.8$. It is seen that the probability of τ_v/τ_0 decays rapidly with τ_v/τ_0 increasing from a small value on the order of w_p to a larger value on the order of τ_0. It is not surprising that most time interval τ_v is on the order of w_p. One contribution to this observation may come from the deformation and fragmentation of thermal plumes by the intense turbulent flow. As a consequence of fragmentation different parts of a single thermal plume, especially sheetlike plumes, may pass through the temperature probe sequentially. The other possible contribution comes

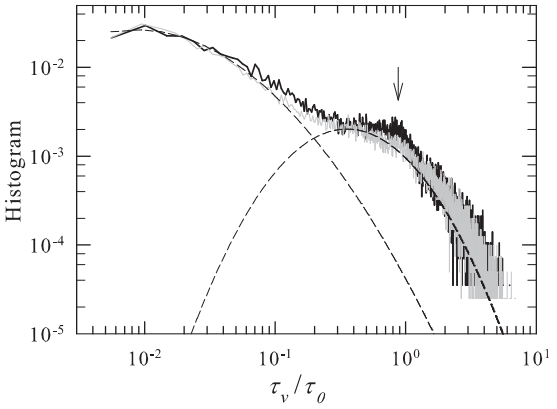

FIG. 5. Histograms of normalized time interval between plumes τ_v/τ_0 at position near the bottom plate (gray line) and near the sidewall (black line) with τ_0 being the large-scale circulation turnover time; the Gaussian fittings are marked as the dashed lines.

from the plumes clusters, where their spacing would be on the same order of plume width. Another obvious feature of the histogram of τ_v/τ_0 is that a hump appears around $\tau_v/\tau_0 = 1$, and this hump is more pronounced for the data measured near the sidewall, which implies that the temperature probe waits for a time period of τ_0 to detect the two successive plumes. This result is consistent with the observation of plume clustering from shadow-graph visualization of the flow field [8,9,29,31]. In another shadow-graph measurement, it was found that the probability density function of plume spacing is a standard log-normal curve [38], which seems different from the present results. But in that measurement, the plume clusters have not been observed, which is different from the present system [8,9,29,31]. Here we fit the histogram of τ_v/τ_0 measured near the sidewall by the combination of two log-normal functions peaked at w_p and τ_0 respectively, shown as dashed lines in Fig. 5. It is seen that the fitting agrees well with experimental data, suggesting that the plume spacing can be described in the form of log-normal distribution as well.

B. Ra dependence of plume properties

To gain insights into the Rayleigh number dependence of plume properties, we measured the temperature signals at both positions over a Ra range from 2×10^8 to 1.85×10^{10}. We have analyzed the temperature traces for different values of β and have found that the scalings of the plume

TABLE I. Scaling exponents of overall temperature fluctuation $T_{\rm rms}/\Delta T$, temperature fluctuation of plumes $T^{\rm pl}_{\rm rms}/\Delta T$, temperature fluctuation of background $T^{bg}_{\rm rms}/\Delta T$, the mean plume spacing $\langle\tau_v\rangle/\tau_0$, and the most probable plume width w_p/τ_0 with respect to Ra, i.e., $\sim{\rm Ra}^\alpha$, for different threshold values of β. The statistical error for all the scaling exponents is ±0.01.

Quantity	Sidewall		Bottom plate	
$T_{\rm rms}/\Delta T$	-0.17		-0.17	
	$\beta=1$	$\beta=2$	$\beta=1$	$\beta=2$
$T^{\rm pl}_{\rm rms}/\Delta T$	-0.18	-0.17	-0.25	-0.25
$T^{bg}_{\rm rms}/\Delta T$	-0.18	-0.18	-0.12	-0.14
$\langle\tau_v\rangle/\tau_0$	-0.24	-0.27	-0.33	-0.35
w_p/τ_0	-0.17	-0.17	-0.23	-0.23

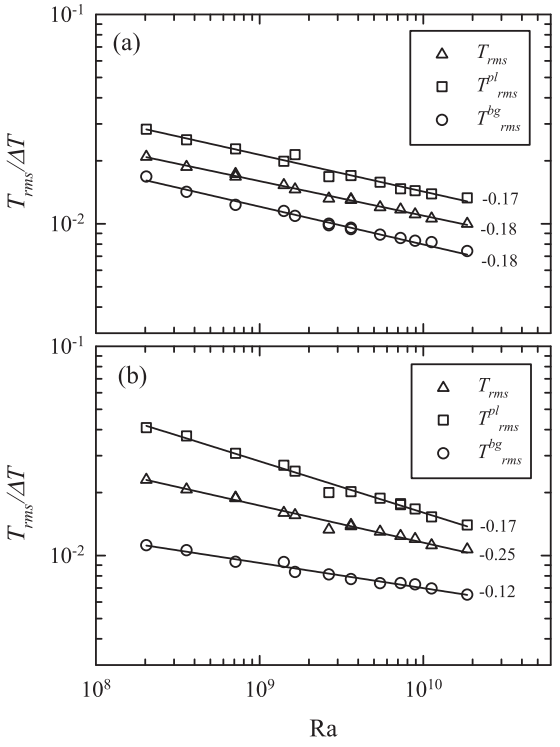

FIG. 6. Ra dependence of the normalized root-mean-square (rms) temperature $T_{\rm rms}/\Delta T$, thermal fluctuation associated with plume $T^{pl}_{\rm rms}/\Delta T$, and that associated with background turbulent fluctuation $T^{bg}_{\rm rms}/\Delta T$ (a) near the sidewall ($x = 20$ mm) and (b) near the bottom plate ($z = 20$ mm). The scaling exponent with respect to Ra is shown nearby each data set.

properties are almost independent of the value of β, as listed in Table I. Below all discussions are merely based on the results at $\beta = 1$.

1. Temperature fluctuation

According to the Grossmann-Lohse (GL) model for turbulent thermal convection [32–35], the overall temperature fluctuation characterized by $T_{\rm rms}$ can be split into two parts, e.g., $T_{\rm rms} = T^{\rm pl}_{\rm rms} + T^{bg}_{\rm rms}$, where $T^{\rm pl}_{\rm rms}$ is the thermal fluctuation of plumes, and $T^{bg}_{\rm rms}$ is the left background thermal fluctuation. The normalized overall temperature fluctuations $T_{\rm rms}/\Delta T$ as a function of Ra near both the sidewall and bottom plate are shown as triangles in Figs. 6(a) and 6(b), respectively. The solid lines in Fig. 6 are a power law fitting to the respective data, which are $T_{\rm rms}/\Delta T = 0.49{\rm Ra}^{-0.17}$ and $T_{\rm rms}/\Delta T = 0.68{\rm Ra}^{-0.17}$. It is seen that the magnitude of $T_{\rm rms}/\Delta T$ near the bottom plate is larger than that near the sidewall, but they have the same Rayleigh number scaling, i.e., $T_{\rm rms}/\Delta T \sim {\rm Ra}^{-0.17}$. Similar results were also reported by Shang *et al.* [49], where it was found that the temperature fluctuations near the bottom plate are larger than those measured near the sidewall. However, the scaling exponent obtained by Shang *et al.* differs from the present experiments. The reason for the different scaling behavior lies in the fact that the measurements done by Shang *et al.* were at varying physical locations where the local heat flux maximizes. In the present case, the measurements are at the fixed locations.

In the literature, temperature fluctuations have been measured mostly at the cell center [50–53]. It has been found that $T_{\rm rms}/\Delta T \sim {\rm Ra}^{-0.145}$ in low-temperature helium gas [50,51] and in water [52] of cylindrical cells, while the scaling exponent is -0.10 in water of a cubic cell [53]. In the theoretical

models, the scaling exponent has been predicted to be $-1/7$ [50,54]. At off-center positions, little work has been reported in this regard except that of Wei *et al.* [55]. They found $T_{\rm rms}/\Delta T \sim {\rm Ra}^{-0.15}$ near the sidewall. The above results suggest that the local temperature fluctuation scaling with respect to Ra might be sensitive to the geometry of the convection cell and is less sensitive to the locations in the cell. The magnitude of temperature fluctuation depends strongly on the location, which is probably due to the different flow dynamics at various locations inside the convection cell.

Based on the the extracted plume signals, like those shown in Fig. 2, thermal fluctuation associated with thermal plumes $T^{\rm pl}_{\rm rms}$, which are characterized by the rms temperature fluctuation from the mean temperature of the total signal $\langle T \rangle$, can be obtained. The Rayleigh number dependence of the normalized thermal fluctuations associated with thermal plumes $T^{\rm pl}_{\rm rms}/\Delta T$ and those associated with the turbulent background $T^{bg}_{\rm rms}/\Delta T$ at sidewall are shown in Fig. 6(a) as squares and circles, respectively. It is seen that $T^{\rm pl}_{\rm rms}/\Delta T$ and $T^{bg}_{\rm rms}/\Delta T$ have the same Ra scaling, i.e., $T^{\rm pl}_{\rm rms}/\Delta T = 0.81{\rm Ra}^{-0.18}$ and $T^{bg}_{\rm rms}/\Delta T = 0.51{\rm Ra}^{-0.18}$. The exponents are very close to that of the overall temperature fluctuation, e.g., -0.17, suggesting that the thermal plumes are rather passive to the intense LSC at the sidewall. One may also notice that the magnitude of $T^{\rm pl}_{\rm rms}/\Delta T$ is larger than that of $T^{bg}_{\rm rms}/\Delta T$.

Near the bottom plate, as shown in Fig. 6(b), $T^{\rm pl}_{\rm rms}/\Delta T$ and $T^{bg}_{\rm rms}/\Delta T$ have different scalings with respect to Ra, i.e., $T^{\rm pl}_{\rm rms}/\Delta T = 4.58{\rm Ra}^{-0.25}$ and $T^{bg}_{\rm rms}/\Delta T = 0.11{\rm Ra}^{-0.12}$. The Ra scaling of $T^{\rm pl}_{\rm rms}/\Delta T$ is much smaller than that of $T_{\rm rms}/\Delta T$, which may due to that the plumes are more active near the plate.

Compared with the GL prediction, for the same Pr, e.g., $T^{\rm pl}_{\rm rms}/\Delta T \sim {\rm Ra}^{-0.10\pm0.01}$ and $T^{bg}_{\rm rms}/\Delta T \sim {\rm Ra}^{-0.13\pm0.03}$ [35], the present experimental results show different scaling exponents except that of the thermal fluctuation due to turbulent background at a position near the bottom plate, which may be a coincidence. We remark that the seemingly reasonable comparison between present results and the GL prediction should be viewed with caution. The decomposition of the volume-averaged thermal dissipation rate into its contribution from the background and that from the thermal plume is a key ingredient of the GL model [32–35]. Following this idea, the theoretically predicted temperature fluctuations associated with the background and those with the plume should also be the globally averaged one. A possible spatial dependence of thermal fluctuations of background and plumes has not been considered in the theoretical model, which may lead to discrepancies between the model prediction and the present local measurements. Additionally, it should be noted that the background thermal fluctuation $T^{bg}_{\rm rms}$ may slightly depend on the value of β used in the plume extraction method, since it still contains some unextracted plume signals when the threshold is larger.

2. Plume width

As discussed in Sec. III A, the most probable plume width w_p is a charateristic feature of thermal plumes in turbulent RBC. We study in this section Ra dependence of w_p, which is shown in Fig. 7. It is seen that w_p/τ_0 decreases with increasing Ra at both positions. The data can be fitted by power laws, i.e., $w_p/\tau_0 = 1.74{\rm Ra}^{-0.24}$ near the bottom plate and $w_p/\tau_0 = 0.37{\rm Ra}^{-0.17}$ near the sidewall. Generally, thermal plumes are deemed as the detached thermal boundary layer, and it is expected that thermal plumes and the thermal boundary layers have the same characteristic length scales [30,35,56,57]. For a better comparison of the two length scales, we also plot the thermal boundary thickness normalized by the cell height H as a function of Ra measured near the bottom plate in Fig. 7 [52]. We can see that w_p/τ_0 is larger than the thermal boundary layer thickness at both locations. In addition, the Ra dependence of w_p/τ_0 is weaker than the thermal boundary layer thickness. It seems reasonable that the plume cap has a larger scale because it is diffusing after detaching from the thermal boundary layer. We note that similar observation was found in a study with high Pr convection, where it is proposed that the thermal boundary layer has a $-1/3$ Ra dependence

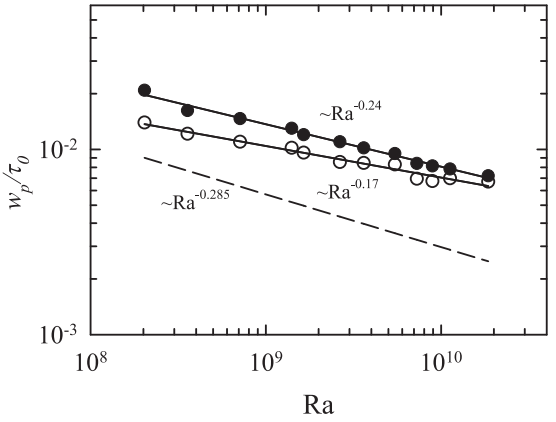

FIG. 7. The most probable plume width w_p/τ_0 as a function of Ra measured at position near the bottom plate (solid circles) and near the sidewall (open circles). The Ra scaling is shown near each data set. The normalized thermal boundary layer thickness, e.g., $\lambda_{\rm th}/H = 2.1{\rm Ra}^{-0.285}$, from Ref. [52] is plotted as dashed line.

[33], and the plume head and radii are found to have -0.14 and -0.21 Ra scaling, respectively [36]. Interestingly, the present results of the plume cap width at moderate Pr are consistent with observations at high Pr.

3. Plume spacing

We study in this section the plume spacing, i.e., the time interval τ_v between thermal plumes. The mean plume spacing normalized by the large-scale circulation turnover time $\langle\tau_v\rangle/\tau_0$ as a function of Ra is shown in Fig. 8. It is seen that $\langle\tau_v\rangle/\tau_0$ decreases monotonically with increasing Ra at both positions. The solid lines in the figure are power law fittings to the data, which are $\langle\tau_v\rangle/\tau_0 = 2.8{\rm Ra}^{-0.32}$ and $\langle\tau_v\rangle/\tau_0 = 4.1{\rm Ra}^{-0.24}$ at positions near the bottom plate and sidewalls respectively. Compared with the previous plume spacing measurement, which shows that the plume spacing has a $1/3$ power law dependence on Ra [37,38,58,59], the present measurements at the bottom plate is consistent with those observations. However, the results at the sidewall differ. One possible reason for the discrepancy may lie in the fact that plumes near the sidewall are relatively

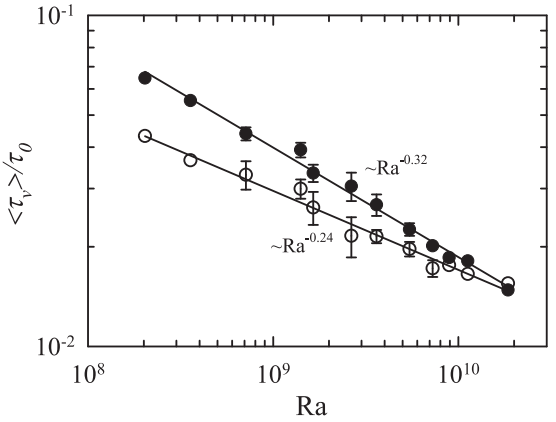

FIG. 8. The averaged normalized plume spacing $\langle\tau_v\rangle/\tau_0$ as a function of Ra measured near the bottom plate (solid circles) and the sidewall (open circles) with τ_0 being the large-scale circulation turnover time. The Ra scaling is shown nearby each data set.

passive. Also the present results suggest a position dependence of the place spacing, which has not been considered in the literature.

IV. CONCLUSIONS

In this paper, we have studied the statistics of thermal plumes in turbulent thermal convection using the temperature time traces measured near both the sidewall and bottom plate in a cylindrical convection cell. Various plume properties, e.g., thermal fluctuations, plume amplitude, plume width, and plume spacing, are studied for a range of Rayleigh number Ra from 2×10^8 to 1.85×10^{10} and Prandtl number 4.3.

At locations near the sidewall and the bottom plate, both plume amplitude A and plume width w are approximately in a log-normal distribution, which are independent of the values of β in the plume extraction method. In particular the histogram of w peaks at the same value for different values of β, suggesting that the most probable plume width w_p is a characteristic scale of thermal plume. Perhaps this scale could correlate to the scaling analysis to learn the energy cascade in thermal turbulence (see, e.g., Ref. [60]). The Ra dependence of w_p/τ_0 is found to be $w_p/\tau_0 = 1.74\mathrm{Ra}^{-0.24}$ near the bottom plate and $w_p/\tau_0 = 0.37\mathrm{Ra}^{-0.17}$ near the sidewall. These scalings exponents are larger than that of thermal boundary layer thickness, e.g., $\lambda_{\mathrm{th}}/H = 2.1\mathrm{Ra}^{-0.285}$ [52] but are consistent with those observed in the high Pr fluid [36].

τ_v represents the plume spacing measured at the fixed location. The histograms of τ_v/τ_0 can be fitted with two log-normal functions, where the respective peaks are located around the most probable plume width w_p and the LSC turnover time τ_0. Near the bottom plate, τ_v/τ_0 is found to scale with Ra as $\langle\tau_v\rangle/\tau_0 \sim \mathrm{Ra}^{-0.32}$, which is consistent with the $-1/3$ scaling in the spatial measurements and numerical simulations [37,38,58,59]. Near the sidewall, where thermal plumes are passively slaved to the LSC, it is found $\langle\tau_v\rangle/\tau_0 \sim \mathrm{Ra}^{-0.24}$. This observation suggests the plume might have different plume spacing behaviors at different locations.

The overall temperature fluctuation at both locations has the same scaling, i.e., $T_{\mathrm{rms}}/\Delta T \sim \mathrm{Ra}^{-0.17}$. The plume fluctuations are $T^{\mathrm{pl}}_{\mathrm{rms}}/\Delta T \sim \mathrm{Ra}^{-0.18}$ and $T^{\mathrm{pl}}_{\mathrm{rms}}/\Delta T \sim \mathrm{Ra}^{-0.25}$ near the sidewall and the bottom plate, respectively. According to the GL predictions, the temperature fluctuation of plumes is $T_{\mathrm{rms}}/\Delta T \sim \mathrm{Ra}^{-0.1}$ in the present parameter range of Ra and Pr [35]. The temperature fluctuations of background near the sidewall and near the bottom plate are, respectively, $T^{bg}_{\mathrm{rms}}/\Delta T \sim \mathrm{Ra}^{-0.18}$ and $T^{bg}_{\mathrm{rms}}/\Delta T \sim \mathrm{Ra}^{-0.12}$. Compared to the GL predictions, where it is predicted that the Ra number scaling varies from -0.11 to -0.16, the present experiments are in disagreement with the GL predictions except for the background temperature fluctuation near the bottom plate, which may be a coincidence.

Finally, the well-defined cliff-ramp structures are commonly observed in many turbulent flows. The method proposed here might be a useful tool to learn some turbulent features in the flow [43–48].

ACKNOWLEDGMENTS

We would like to thank H.-D. Xi and Q. Zhou for illuminating discussions. This work was supported by the Hong Kong Research Grants Council through General Research Fund Grants No. CUHK 403712 and No. CUHK 404513; and S.-Q.Z. was partially supported by the Strategic Priority Research Program of the Chinese Academy of Sciences through Grant No. XDA11030302.

[1] M. Rieutord and J.-P. Zahn, Turbulent plumes in stellar convective envelopes, Astron. Astrophys. **296**, 127 (1995).

[2] A. M. Jellinek and M. Manga, Links between long-lived hot spots, mantle plumes, D″, and plate tectonics, Rev. Geophys. **42**, RG3002 (2004).

[3] G. Ahlers, S. Grossmann, and D. Lohse, Heat transfer and large-scale dynamics in turbulent Rayleigh-Bénard convection, Rev. Mod. Phys. **81**, 503 (2009).
[4] D. Lohse and K.-Q. Xia, Small-scale properties of turbulent Rayleigh-Bénard convection, Annu. Rev. Fluid Mech. **42**, 335 (2010).
[5] F. Chillà and J. Schumacher, New perspectives in turbulent Rayleigh-Bénard convection, Eur. Phys. J. E **35**, 58 (2012).
[6] K.-Q. Xia, Experimental studies of turbulent Rayleigh-Bénard convection, in *Advances in Turbulence XII: Proceedings of the 12th EUROMECH European Turbulence Conference*, edited by B. Eckhardt (Springer, Berlin, 2009), p. 471.
[7] K.-Q. Xia, Current trends and future directions in turbulent thermal convection, Theor. Appl. Mech. Lett. **3**, 052001 (2013).
[8] H.-D. Xi, S. Lam, and K.-Q. Xia, From laminar plumes to organized flows: The onset of large-scale circulation in turbulent thermal convection, J. Fluid Mech. **503**, 47 (2004).
[9] X.-D. Shang, X.-L. Qiu, P. Tong, and K.-Q. Xia, Measured Local Heat Transport in Turbulent Rayleigh-Bénard Convection, Phys. Rev. Lett. **90**, 074501 (2003).
[10] X.-D. Shang, X.-L. Qiu, P. Tong, and K.-Q. Xia, Measurements of the local convective heat flux in turbulent Rayleigh-Bénard convection, Phys. Rev. E **70**, 026308 (2004).
[11] W. V. R. Malkus, Discrete transitions in turbulent convection, Proc. R. Soc. London A **225**, 185 (1954).
[12] L. N. Howard, Convection at high Rayleigh number, in *Applied Mechanics*, Proceedings of the Eleventh International Congress of Applied Mechanics Munich (Germany) 1964 (Springer, Berlin, 1966), p. 1109.
[13] G. Zocchi, E. Moses, and A. Libchaber, Coherent structures in turbulent convection, an experimental study, Physica A (Amsterdam) **166**, 387 (1990).
[14] A. Belmonte and A. Libchaber, Thermal signature of plumes in turbulent convection: The skewness of the derivative, Phys. Rev. E **53**, 4893 (1996).
[15] S.-Q. Zhou and K.-Q. Xia, Plume Statistics in Thermal Turbulence: Mixing of an Active Scalar, Phys. Rev. Lett. **89**, 184502 (2002).
[16] K. Julien, S. Legg, J. McWilliams, and J. Werne, Plumes in rotating convection. Part 1. Ensemble statistics and dynamical balances, J. Fluid Mech. **391**, 151 (1999).
[17] E. S. C. Ching, H. Guo, X.-D. Shang, P. Tong, and K.-Q. Xia, Extraction of Plumes in Turbulent Thermal Convection, Phys. Rev. Lett. **93**, 124501 (2004).
[18] O. Shishkina and C. Wagner, Analysis of thermal dissipation rates in turbulent Rayleigh-Bénard convection, J. Fluid Mech. **546**, 51 (2006).
[19] O. Shishkina and C. Wagner, Analysis of sheet-like thermal plumes in turbulent Rayleigh-Bénard convection, J. Fluid Mech. **599**, 383 (2008).
[20] S.-D. Huang, M. Kaczorowski, R. Ni, and K.-Q. Xia, Confinement-Induced Heat-Transport Enhancement in Turbulent Thermal Convection, Phys. Rev. Lett. **111**, 104501 (2013).
[21] Y.-C. Xie, S.-D. Huang, D. Funfschilling, X.-M. Li, R. Ni, and K.-Q. Xia, Effects of polymer additives in the bulk of turbulent thermal convection, J. Fluid Mech. **784**, R3 (2015).
[22] J. Zhang and A. Libchaber, Periodic Boundary Motion in Thermal Turbulence, Phys. Rev. Lett. **84**, 4361 (2000).
[23] D. Funfschilling and G. Ahlers, Plume Motion and Large-Scale Circulation in a Cylindrical Rayleigh-Bénard Cell, Phys. Rev. Lett. **92**, 194502 (2004).
[24] Q. Zhou, C. Sun, and K.-Q. Xia, Morphological Evolution of Thermal Plumes in Turbulent Rayleigh-Bénard Convection, Phys. Rev. Lett. **98**, 074501 (2007).
[25] Q. Zhou and K.-Q. Xia, Physical and geometrical properties of thermal plumes in turbulent Rayleigh-Bénard convection, New J. Phys. **12**, 075006 (2010).
[26] J. Bosbach, S. Weiss, and G. Ahlers, Plume Fragmentation by Bulk Interactions in Turbulent Rayleigh-Bénard Convection, Phys. Rev. Lett. **108**, 054501 (2012).
[27] X.-L. Qiu and P. Tong, Temperature oscillations in turbulent Rayleigh-Bénard convection, Phys. Rev. E **66**, 026308 (2002).
[28] X.-L. Qiu and P. Tong, Large-scale velocity structures in turbulent thermal convection, Phys. Rev. E **64**, 036304 (2001).

[29] A. Parodi, J. von Hardenberg, G. Passoni, A. Provenzale, and E. A. Spiegel, Clustering of Plumes in Turbulent Convection, Phys. Rev. Lett. **92**, 194503 (2004).
[30] E. P. van der Poel, R. Verzicco, S. Grossmann, and D. Lohse, Plume emission statistics in turbulent Rayleigh-Bénard convection, J. Fluid Mech. **772**, 5 (2015).
[31] A. Bershadskii, J. J. Niemela, A. Praskovsky, and K. R. Sreenivasan, "Clusterization" and intermittency of temperature fluctuations in turbulent convection, Phys. Rev. E **69**, 056314 (2004).
[32] S. Grossmann and D. Lohse, Scaling in thermal convection: A unifying theory, J. Fluid Mech. **407**, 27 (2000).
[33] S. Grossmann and D. Lohse, Thermal Convection for Large Prandtl Numbers, Phys. Rev. Lett. **86**, 3316 (2001).
[34] S. Grossmann and D. Lohse, Prandtl and Rayleigh number dependence of the Reynolds number in turbulent thermal convection, Phys. Rev. E **66**, 016305 (2002).
[35] S. Grossmann and D. Lohse, Fluctuations in turbulent Rayleigh-Bénard convection: The role of plumes, Phys. Fluids **16**, 4462 (2004).
[36] C. Lithgow-Bertelloni, M. A. Richards, C. P. Conrad, and R. W. Griffiths, Plume generation in natural thermal convection at high Rayleigh and Prandtl numbers, J. Fluid Mech. **434**, 1 (2001).
[37] E. M. Parmentier and C. Sotin, Three-dimensional numerical experiments on thermal convection in a very viscous fluid: Implications for the dynamics of a thermal boundary layer at high Rayleigh number, Phys. Fluids **12**, 609 (2000).
[38] B. A. Puthenveettil and J. H. Arakeri, Plume structure in high-Rayleigh-number convection, J. Fluid Mech. **542**, 217 (2005).
[39] S.-Q. Zhou and K.-Q. Xia, Scaling Properties of the Temperature Field in Convective Turbulence, Phys. Rev. Lett. **87**, 064501 (2001).
[40] E. Moses, G. Zocchi, I. Procaccia, and A. Libchaber, The dynamics and interaction of laminar thermal plumes, Europhys. Lett. **14**, 55 (1991).
[41] E. Moses, G. Zocchi, and A. Libchaberii, An experimental study of laminar plumes, J. Fluid Mech. **251**, 581 (1993).
[42] R. A. Antonia, Conditional sampling in turbulence measurement, Annu. Rev. Fluid Mech. **13**, 131 (1981).
[43] T. Kikas, H. Ishida, P. J. W. Roberts, D. R. Webster, and J. Janata, Virtual plume, Electroanalysis **12**, 974 (2000).
[44] J. Zhang, X. L. Wu, and N. Rashidnia, Thermal radiation and thickness fluctuations in freely suspended liquid films, Phys. Fluids **18**, 085110 (2006).
[45] P. G. Mestayer, C. H. Gibson, M. F. Coantic, and A. S. Patel, Local anisotropy in heated and cooled turbulent boundary layers, Phys. Fluids **19**, 1279 (1976).
[46] C. H. Gibson, C. A. Friehe, and S. O. McConnell, Structure of sheared turbulent fields, Phys. Fluids **20**, S156 (1977).
[47] Z. Warhaft, Passive scalars in turbulent flows, Annu. Rev. Fluid Mech. **32**, 203 (2000).
[48] F. Moisy, H. Willaime, J. S. Andersen, and P. Tabeling, Passive Scalar Intermittency in Low Temperature Helium Flows, Phys. Rev. Lett. **86**, 4827 (2001).
[49] X.-D. Shang, P. Tong, and K.-Q. Xia, Scaling of the Local Convective Heat Flux in Turbulent Rayleigh-Bénard Convection, Phys. Rev. Lett. **100**, 244503 (2008).
[50] B. Castaing, G. Gunaratne, F. Heslot, L. Kadanoff, A. Libchaber, S. Thomae, X.-Z. Wu, S. Zaleski, and G. Zanetti, Scaling of hard thermal turbulence in Rayleigh-Bénard convection, J. Fluid Mech. **204**, 1 (1989).
[51] J. J. Niemela, L. Skrbek, K. R. Sreenivasan, and R. J. Donnelly, Turbulent convection at very high Rayleigh numbers, Nature (London) **404**, 837 (2000).
[52] S.-L. Lui and K.-Q. Xia, Spatial structure of the thermal boundary layer in turbulent convection, Phys. Rev. E **57**, 5494 (1998).
[53] Z. A. Daya and R. E. Ecke, Does Turbulent Convection Feel the Shape of the Container? Phys. Rev. Lett. **87**, 184501 (2001).
[54] B. I. Shraiman and E. D. Siggia, Heat transport in high-Rayleigh-number convection, Phys. Rev. A **42**, 3650 (1990).

[55] P. Wei, R. Ni, and K.-Q. Xia, Enhanced and reduced heat transport in turbulent thermal convection with polymer additives, Phys. Rev. E **86**, 016325 (2012).
[56] A. Belmonte, A. Tilgner, and A. Libchaber, Temperature and velocity boundary layers in turbulent convection, Phys. Rev. E **50**, 269 (1994).
[57] J. Werne, Plume model for the boundary-layer dynamics in hard turbulence, Phys. Rev. E **49**, 4072 (1994).
[58] S. A. Theerthan and J. H. Arakeri, A model for near-wall dynamics in turbulent Rayleigh-Bénard convection, J. Fluid Mech. **373**, 221 (1998).
[59] S. A. Theerthan and J. H. Arakeri, Planform structure and heat transfer in turbulent free convection over horizontal surfaces, Phys. Fluids **12**, 884 (2000).
[60] A. S. Monin and A. M. Yaglom, *Statistical Fluid Mechanics: Mechanics of Turbulence* (MIT Press, Cambridge, MA, 1971).